
Augmentation-aware Self-supervised Learning with Guided Projector

Marcin Przewięzlikowski^{1,2,3} * **Mateusz Pyla^{1,2,3}** **Bartosz Zieliński^{1,3}**
Bartłomiej Twardowski^{3,4} **Jacek Tabor¹** **Marek Śmieja¹**
¹ Jagiellonian University, Faculty of Mathematics and Computer Science
² Jagiellonian University, Doctoral School of Exact and Natural Sciences
³ IDEAS NCBR ⁴ Universitat Autònoma Barcelona

Abstract

Self-supervised learning (SSL) is a powerful technique for learning robust representations from unlabeled data. By learning to remain invariant to applied data augmentations, methods such as SimCLR and MoCo are able to reach quality on par with supervised approaches. However, this invariance may be harmful to solving some downstream tasks which depend on traits affected by augmentations used during pretraining, such as color. In this paper, we propose to foster sensitivity to such characteristics in the representation space by modifying the projector network, a common component of self-supervised architectures. Specifically, we supplement the projector with information about augmentations applied to images. In order for the projector to take advantage of this auxiliary guidance when solving the SSL task, the feature extractor learns to preserve the augmentation information in its representations. Our approach, coined **Conditional Augmentation-aware Self-supervised Learning (CASSLE)**, is directly applicable to typical joint-embedding SSL methods regardless of their objective functions. Moreover, it does not require major changes in the network architecture or prior knowledge of downstream tasks. In addition to an analysis of sensitivity towards different data augmentations, we conduct a series of experiments, which show that CASSLE improves over various SSL methods, reaching state-of-the-art performance in multiple downstream tasks.²

1 Introduction

Artificial neural networks have proven to be a successful family of models in several domains, including, but not limited to, computer vision [29], natural language processing [10], and solving problems at the human level with reinforcement learning [42]. This success is attributed largely to their ability to learn useful feature representations [27] without additional effort for input signals preparation. However, training large deep learning models requires extensive amounts of data, which can be costly to prepare, especially when human annotation is needed [3, 33].

High-quality image representations can be acquired without relying on explicitly labeled data by utilizing self-supervised learning (SSL). A self-supervised model is trained once on a large dataset without labels and then transferred to different downstream tasks. Initially, self-supervised methods addressed well-defined pretext tasks, such as predicting rotation [26] or determining patch position [21]. Recent studies in SSL proposed contrastive methods learning representations that remain invariant when subjected to various data augmentations [32, 13, 64] leading to impressive results that have greatly diminished the disparity with representations learned in a supervised way [11].

*Corresponding author: marcin.przewiezlikowski@doctoral.uj.edu.pl

²We share our codebase at <https://github.com/gmum/CASSLE>.

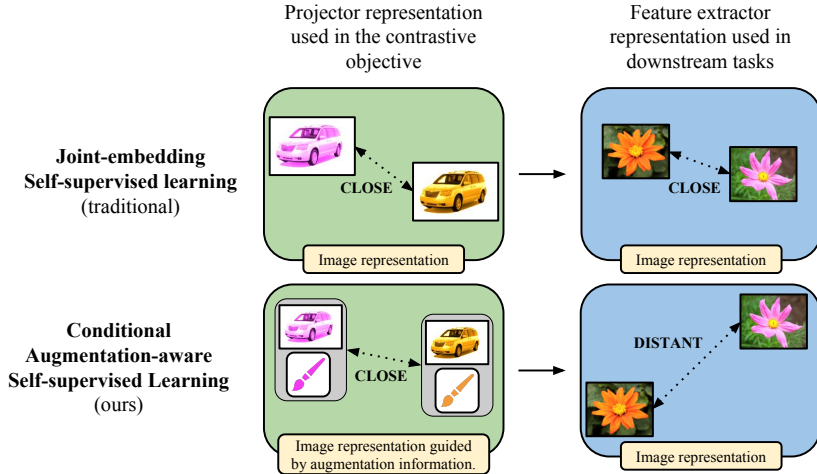


Figure 1: In the traditional self-supervised setting, contrastive loss minimization pulls the representations of augmented image views closer in the latent space of the projector (left). This may also reduce the distance between their feature extractor representations (right). Thus, the representation becomes more invariant to augmentation-induced perturbations, which may hinder the performance on downstream tasks. In contrast, the self-supervised objective of CASSLE draws together joint representations of images and their augmentations in the projector space (bottom row). By conditioning the projector with augmentation information, image representations retain more sensitivity to perturbations in the feature extractor space. This proves to be beneficial when solving downstream tasks.

Nevertheless, contrastive methods may perform poorly when a particular downstream task relies on features affected by augmentation [66]. For example, color jittering can result in a representation space invariant to color shifts, which would be detrimental to the task of flower classification (see Figure 1). Without prior knowledge of possible downstream tasks, this effect is hard to mitigate in contrastive learning [58, 66]. Solutions for retaining information about used data augmentations in the feature extractor representation include forcing it explicitly with a modified training scheme [66, 37, 67], or by preparing a feature extractor to be adapted to a specific downstream task, e.g., with hypernetworks [12]. However, these approaches often involve significant modifications either to the contrastive model architecture [66], training procedure [37, 67], or costly training of additional models [12].

In this work, we propose a new method called **Conditional Augmentation-aware Self-supervised Learning (CASSLE)** that mitigates augmentation invariance of representation without neither major changes in network architecture or modifications to the self-supervised training objective. We propose to use the augmentation information during the SSL training as additional guidance for the projector network. This encourages the feature extractor network to retain information about augmented image features in its representation. CASSLE can be applied to any joint-embedding SSL method regardless of its objective, provided that it utilizes a projector network [14, 13, 64, 70, 15]. The outcome is a general-purpose, augmentation-aware encoder that can be directly used for any downstream task. CASSLE presents improved results in comparison to other augmentation-aware SSL methods, improving transferability to downstream tasks where invariance of the model representation for specific data changes could be harmful.

The main contributions of our work are threefold:

- We propose a simple yet effective method for Conditional Augmentation-aware Self-supervised Learning (CASSLE). Using our guided projector enables preserving more information about augmentations in representations than in existing methods.
- CASSLE is a general modification that can be directly applied to existing joint-embedding SSL approaches without introducing additional objectives and major changes in the network architecture.
- In a series of experiments we demonstrate that CASSLE reaches state-of-the-art performance with different SSL methods for robust representation learning and improves upon the performance of previous augmentation-aware approaches. Furthermore, our analysis indicates that CASSLE learns representations with increased augmentation sensitivity compared to other approaches.

2 Related work

Self-supervised learning (SSL) is a paradigm of learning representations from unlabeled data that can later be used for downstream tasks defined by human annotations [2, 4]. Despite learning artificial *pretext tasks*, instead of data-defined ones, SSL models have achieved tremendous success in a plethora of domains [20, 63, 56, 7]. This includes computer vision, where a variety of pretext tasks has been proposed [21, 71, 45, 26]. However, arguably the most prominent and successful SSL technique to emerge in recent years is training of joint-embedding models for augmentation invariance [6, 60], defined by objectives such as contrastive InfoNCE loss [32, 13, 14], self-distillation [30, 13, 46] or Canonical Correlation Analysis [39, 70, 5]. Those objectives are often collectively referred to as *contrastive objectives* [59, 4]. A common component of joint-embedding architectures is the *projector network*, which maps representations of the feature extractor into the space where the contrastive objective is imposed [13, 14]. The usefulness of the projector has been explained through the lens of transfer learning, where it is often better to transfer intermediate network representations, to reduce the biases from the pretraining task [68, 8]. The projector also helps to mitigate the noisy data augmentations and enforces some degree of pairwise independence of image features [4, 41].

Augmentation invariance of self-supervised models is a natural consequence of training them with contrastive objectives and it is crucial to choose such augmentations which will allow to form useful representations [13]. While a common set of augmentations demonstrated to typically work well on natural images in SSL has been established in the literature [32, 13, 64, 39, 72], the optimal choice of augmentations varies between specific tasks [58, 23]. Xiao et. al. find that augmentation invariance can hinder the performance of the model on downstream tasks which require attention to precisely those traits that it had been previously trained to be invariant to [66]. This inspired several techniques of retaining augmentation-specific information in joint-embedding models, such as projectors sensitive to different augmentation types [66, 23], adding an objective of explicit prediction of augmentation parameters [37], weighing the contrastive objective with the augmentation strength [67], as well as task-specific pretraining [52, 61]. The above approaches produce general-purpose feature extractors which can be transferred to downstream tasks without further tuning of their parameters. However, they often involve complex modifications either to the SSL model architecture [66], training procedure [37, 67], or simply tedious task-specific pretraining [61]. Another line of work proposes to train Hypernetworks [28] which produce feature extractors invariant to chosen subsets of augmentations – a more elastic, but considerably harder to train approach [12]. Following [66, 37], we produce a general-purpose feature extractor and utilize augmentation information similarly to [37, 12]. Contrary to the above methods, we inject the information about the applied augmentations directly into the projector and make no modification either to the contrastive objective or the feature extractor.

3 Method

In this section, we present our approach, Conditional Augmentation-aware Self-supervised learning (CASSLE). Section 3.1 provides a background on joint-embedding self-supervised methods and their limitations. Section 3.2 explains the essence of CASSLE and how it leverages augmentation information to improve the quality of learned representations. Section 3.3 describes the details of CASSLE and its implementation.

3.1 Preliminaries

A typical contrastive framework used in self-supervised learning consists of an augmentation function t_ω and two networks: feature extractor f and projector π . Let $\mathbf{v}_1 = t_{\omega_1}(\mathbf{x})$, $\mathbf{v}_2 = t_{\omega_2}(\mathbf{x})$ be two augmentations of a sample $\mathbf{x} \sim X$ parameterized by $\omega_1, \omega_2 \sim \Omega$. The feature extractor maps them into the embedding space, which is the representation used in downstream tasks. To make the representation invariant to data augmentations, $\mathbf{e}_1 = f(\mathbf{v}_1)$ is forced to be similar to $\mathbf{e}_2 = f(\mathbf{v}_2)$ ³. Instead of imposing similarity constraints directly on the embedding space of f , we use a projector π , which transforms the embeddings into target space for applying the contrastive loss \mathcal{L} . This trick, known as *Guillotine Regularization*, helps the feature extractor to better generalize to downstream tasks, due to f not being directly affected by \mathcal{L} [68, 13, 14, 8].

³While contrastive objectives such as InfoNCE [60] regularize the representation using negative pairs, we omit them from our notation for the sake of brevity.

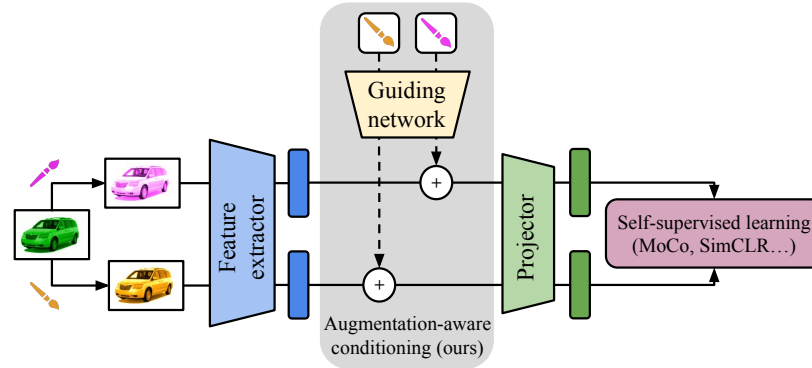


Figure 2: Overview of CASSLE. We extend the typical self-supervised learning approaches by incorporating the information of augmentations applied to images into the projector network. The Guiding network infers the representations of augmentations and passes them to the projector network as conditional inputs. In CASSLE, the SSL objective is thus imposed on joint representations of images and the augmentations that had been applied to them. This way, CASSLE enables the feature extractor to be more aware of augmentations than the methods that do not condition the projector network.

Minimizing $\mathcal{L}(\pi(\mathbf{e}_1), \pi(\mathbf{e}_2))$ directly leads to reducing the distance between embeddings $\pi(\mathbf{e}_1)$ and $\pi(\mathbf{e}_2)$. However, \mathcal{L} still indirectly encourages intermediate network representations (including the output of the feature extractor f) to also conform to the contrastive objective to some extent, which means that the feature extractor tends to erase the information about augmentation from its output representation. This behavior may however be detrimental for certain downstream tasks (see Figures 1 and 4), which rely on features affected by augmentations. For instance, learning invariance to color jittering through standard contrastive methods may lead to degraded performance on the downstream task of flower recognition is not a color-invariant task [58, 66]. Consequently, the success of typical SSL approaches depends critically on a careful choice of augmentations used for model pretraining [13, 58].

3.2 CASSLE

To overcome the above limitations of SSL, we guide the feature extractor to encode the information about augmentations in its output representation. In consequence, the obtained representation will be more informative for downstream tasks which depend on features modified by augmentations.

CASSLE achieves this goal by conditioning the projector π on the parameters of augmentations used to perturb the input image. Specifically, we introduce the Guiding network γ which transforms augmentation parameters $\omega \sim \Omega$ into *augmentation embeddings* $\mathbf{g} = \gamma(\omega)$. Moreover, we modify π to transform the joint image and augmentation representations (\mathbf{e}, \mathbf{g}) into the space where the objective \mathcal{L} is imposed. We do not alter the \mathcal{L} itself; instead, training relies on minimizing the contrastive loss \mathcal{L} between $\pi(\mathbf{e}_1, \omega_1)$ and $\pi(\mathbf{e}_2, \omega_2)$. Thus, π learns to draw \mathbf{e}_1 and \mathbf{e}_2 together in its representation space *on condition of* \mathbf{g}_1 and \mathbf{g}_2 . We visualize the architecture of CASSLE in Figure 2.

Let us explain why CASSLE reduces the detrimental effect of augmentations on the representations of feature extractor f . If π minimizes \mathcal{L} on embeddings enriched with information about augmentation, then f is encouraged to preserve augmentation information in its representation. Intuitively, by retaining the information about augmented features in feature extractor, we facilitate the image and augmentation representations to counter one another in the projector. Without this guidance, the feature extractor and projector could be considered as a single network which could erase information about augmentation at any intermediate layer. Since CASSLE guides the feature extractor to encode the augmented features, its performance is not as vulnerable to incorrectly selected augmentations as in the vanilla SSL approaches. In particular, CASSLE pretrained with color jittering can still be used in the downstream task of flower recognition, while for vanilla approaches this augmentation should be prohibited.

CASSLE can be applied to a variety of joint-embedding methods, as the only modification it makes is changing the projector network to utilize the additional input produced by the guiding network. We do not modify any additional aspects of the extended self-supervised approaches, such as objective functions, which is appealing from a practical perspective. Last but not least, the architecture of the feature extractor in CASSLE is not affected by the introduced augmentation guidance. Since we only modify the input to the projector, which is discarded after the pretraining, the feature extractor can be directly used in downstream tasks similar to vanilla SSL techniques.

3.3 Practical implementation of the guidance mechanism

We construct augmentation information ω by concatenating vectors ω^{aug} describing the parameters of each augmentation type [37]. In this work, we focus on a set of augmentations used commonly in the literature [13, 14, 64], listed below along with descriptions of their respective parameters ω^{aug} :

- **random cropping** – $\omega^c \in [0, 1]^4$ describes the normalized coordinates of cropped image center and cropping sizes.
- **color jittering** – $\omega^j \in [0, 1]^4$ describes the normalized intensities of brightness, contrast, saturation, and hue adjustment.
- **Gaussian blurring** – $\omega^b \in [0, 1]$ is the standard deviation of the Gaussian filter used during the blurring operation.
- **random horizontal flipping** – $\omega^f \in \{0, 1\}$ indicates whether the image has been flipped.
- **random grayscaling** – $\omega^g \in \{0, 1\}$ indicates whether the image has been reduced to grayscale.

To enhance the projector’s awareness of the color changes in the augmented images, we additionally enrich ω with information about **color difference** – $\omega^d \in [0, 1]^3$, which is computed as the difference between the mean values of color channels of the image before and after the color jittering operation. We empirically remonstrate that inclusion of ω^d in ω improves the performance of CASSLE (see Section 4.4).

Afterwards, the Guiding network γ , transforms ω into augmentation embeddings \mathbf{g} . For the architecture of γ we choose the Multi-layer Perceptron. We condition the projector π with \mathbf{g} by concatenating \mathbf{g} to the image embeddings \mathbf{e} before feeding them to π . We also explore other alternatives for combining \mathbf{g} and \mathbf{e} for conditioning π (see Section 4.4)

4 Experiments

In Section 4.1, we evaluate CASSLE’s performance on downstream tasks such as classification, regression, object detection, and image retrieval⁴. In Section 4.2, we analyze CASSLE’s sensitivity to augmentations and conditioning, as well as its effect on the process of contrastive pretraining in Section 4.3. Finally, we discuss the choice of hyperparameters of CASSLE in Section 4.4. In all experiments, unless specified otherwise, we utilize the ResNet-50 architecture [29] and conduct the self-supervised pretraining on ImageNet-100 - a 100-class subset of the ILSVRC dataset [53] used commonly in the literature [58, 66, 37, 12]. We use the standard set of augmentations including horizontal flipping, random cropping, grayscaling, color jittering and Gaussian blurring [32, 37, 30]. For consistency in terms of hyperparameters, we follow [37] for MoCo-v2 and SimSiam, and [12] for SimCLR. We describe additional details of training and evaluation in the supplementary material.

4.1 Evaluation on downstream tasks

We begin the experimental analysis by addressing the most fundamental question – how does CASSLE impact the ability of models to generalize? In order to answer it, we evaluate models pretrained via CASSLE and other self-supervised techniques on a variety of downstream visual tasks, such as classification, regression, object detection, and image retrieval.

⁴We compare CASSLE to a number of recently proposed methods [66, 37, 12]. We report the performance of those methods from the literature [58, 66, 37, 12], given that the code for [66] and [12] was not made available at the time of writing. As for the results of baseline SSL models and AugSelf [37], we report their results from the literature except when our runs of those methods yielded results different by at least 2 pp. We mark such cases with †.

Table 1: Linear evaluation on downstream classification and regression tasks. CASSLE consistently improves representations formed by vanilla SSL approaches and performs better or comparably to other techniques of increasing sensitivity to augmentations [66, 37, 12].

Method	C10	C100	Food	MIT	Pets	Flowers	Caltech	Cars	FGVCA	DTD	SUN	CUB	300W
<i>SimCLR</i> [13]													
Vanilla	81.80	61.40	56.59 [†]	61.26 [†]	69.10	81.58 [†]	75.95 [†]	31.20 [†]	38.68 [†]	64.99 [†]	46.37 [†]	28.87 [†]	88.47 [†]
AugSelf [37] [†]	84.30	63.47	60.76	63.43	71.86	86.59	79.88	36.56	42.90	66.59	48.84	34.46	88.79
AI [12]	83.90	63.10	–	–	69.50	68.30	74.20	–	–	53.70	–	38.60	88.00
CASSLE	85.61	64.09	61.00	63.58	71.43	85.98	80.62	37.97	42.26	67.07	49.42	33.91	89.05
<i>MoCo-v2</i> [32, 14]													
Vanilla	84.60	61.60	59.67	61.64	70.08	82.43	77.25	33.86	41.21	64.47	46.50	32.20	88.77 [†]
AugSelf [37]	85.26	63.90	60.78	63.36	73.46	85.70	78.93	37.35	39.47	66.22	48.52	37.00	89.49 [†]
AI [12]	81.30	64.60	–	–	74.00	81.30	78.90	–	–	68.80	–	41.40	90.00
LooC [66]	–	–	–	–	–	–	–	–	–	–	–	39.60	–
CASSLE	86.32	65.29	61.93	63.86	72.86	86.51	79.63	38.82	42.03	66.54	49.25	36.22	88.93
<i>Barlow Twins</i> [70]													
Vanilla [†]	85.90	66.10	59.41	61.72	72.30	87.13	81.95	41.54	44.40	65.85	49.18	35.02	89.04
AugSelf [37] [†]	87.28	66.98	60.52	63.96	72.11	86.68	81.73	39.88	44.23	65.21	47.71	37.02	88.88
CASSLE	87.03	67.27	62.19	65.08	72.75	87.99	82.56	41.68	46.63	66.31	50.09	38.25	89.52
<i>SimSiam</i> [64]													
Vanilla	86.89	66.33	61.48	65.75	74.69	88.06	84.13	48.20	48.63	65.11	50.60	38.40	89.01
AugSelf [37]	88.80	70.27	65.63	67.76	76.34	90.70	85.30	47.52	49.76	67.29	52.28	45.30	92.84
CASSLE	87.38	67.36	63.27	66.84	75.02	88.95	84.86	48.51	49.35	66.81	51.62	39.47	89.37
<i>MoCo-v3</i> [32, 15] (ViT-Small feature extractor [22] pretrained on the full ImageNet dataset.)													
Vanilla [†]	83.17	62.40	56.15	53.28	62.29	81.48	69.63	28.63	32.84	57.18	42.16	35.00	87.42
AugSelf [37] [†]	84.25	64.12	58.28	56.12	63.93	83.13	72.45	29.64	32.54	60.27	43.22	37.16	87.85
CASSLE	85.13	64.67	57.30	55.90	63.88	82.42	73.53	30.92	35.91	58.24	43.37	36.09	88.53

Linear evaluation We evaluate the performance of pretrained networks on the downstream tasks of classification on a wide array of datasets: CIFAR10/100 (C10/100) [36], Food101 (Food) [9], MIT67 (MIT) [51], Oxford-IIIT Pets (Pets) [48], Oxford Flowers-102 (Flowers) [44], Caltech101 (Caltech) [25], Stanford Cars (Cars) [35], FGVC-Aircraft (FGVCA) [40], Describable Textures (DTD) [17], SUN-397 (SUN) [65], as well as regression on the 300 Faces In-the-Wild (300W) dataset [55]. We follow the linear evaluation protocol [34, 13, 37], described in detail in the supplementary material. We evaluate multiple self-supervised methods extended with CASSLE, as well as other recently proposed extensions which increase sensitivity to augmentations [37, 66, 12]. The results, averaged over 3 random seeds, are reported in Table 1. We find that in the vast majority of cases, CASSLE improves the performance of vanilla joint-embedding methods. Moreover, in the case of InfoNCE-based (SimCLR, MoCo), and CCA-based (Barlow Twins) approaches, CASSLE generally achieves better downstream results than the other SSL extensions [37, 12]. On the other hand, CASSLE gives a lower performance boost to SimSiam [64] than AugSelf [37], nevertheless improving the vanilla approach.

Object detection We next evaluate the pretrained networks on a more challenging task of object detection on the VOC 2007 dataset [24]. We follow the training scheme of [32, 14], except that we only train the object detector modules and keep the feature extractor parameters fixed during training for detection to better compare the pretrained representations. We report the Average Precision (AP) [38] of models pretrained through MoCo-v2 and SimCLR [13] with AugSelf [37] and CASSLE extensions in Table 2. The compared approaches yield similar results, with CASSLE representation slightly surpassing the vanilla methods and AugSelf.

Table 2: Average Precision of object detection on VOC dataset [24, 38]. CASSLE extension of MoCo-v2 and SimCLR outperforms the vanilla approaches and AugSelf extension by a small margin.

Method	<i>MoCo-v2</i>	<i>SimCLR</i>
Vanilla	45.12	44.78
AugSelf [37]	45.20	44.44
CASSLE	45.90	45.02

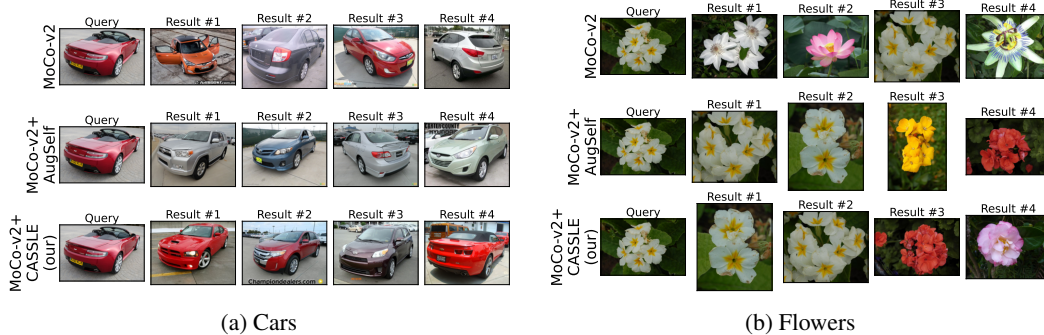


Figure 3: Example of image retrieval performed by feature extractors pretrained via MoCo-v2 as well as AugSelf [37] and CASSLE on Cars and Flowers images. The CASSLE feature extractor retrieves images with more consistent color scheme and object shape than other approaches.

Image retrieval Finally, we benchmark the pretrained models on the task of image retrieval. We select query images from the Cars and Flowers datasets and find four examples closest to queries in terms of cosine similarities of feature extractor representations. We compare the images retrieved by MoCo-v2, AugSelf [37] and CASSLE in Figure 3. CASSLE selects pictures of cars that are the most consistent in terms of color. In the case of flowers, the nearest neighbor retrieved by the vanilla model is a different species than that of the query image, whereas both CASSLE and AugSelf select the first two nearest neighbors from the same species but then retrieve images of flowers with similar shapes, but different colors. This again indicates greater reliability of features learned by CASSLE.

4.2 Analysis of representations formed by CASSLE

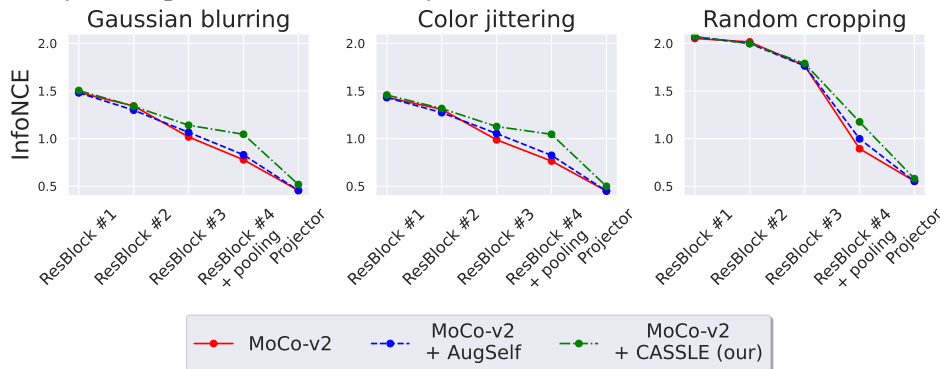


Figure 4: A comparison of InfoNCE loss measured on different kinds of augmentations at subsequent stages of the ResNet-50 and projectors pretrained by vanilla, AugSelf [37] and CASSLE variants of MoCo-v2. Feature extractor representation of CASSLE yields higher InfoNCE values which suggests that it is more susceptible to augmentations.

Sensitivity to augmentations We investigate the awareness of augmentation-induced data perturbations in the intermediate and final representations of pretrained networks. As a proxy metric for measuring this, we choose the InfoNCE loss [60, 13]. The value of InfoNCE is high if embeddings of pairs of augmented images are less similar to one another than to embeddings of unrelated images, and low if positive pairs of embeddings are on average separated correctly, and thus, the given representation is invariant to augmentations. We report the mean InfoNCE loss values under different augmentation types at subsequent stages of ResNet-50 and projectors of MoCo-v2, AugSelf [37] and CASSLE in Figure 4.

In all networks, the augmentation awareness decreases gradually throughout the feature extractor and projector stages. In CASSLE, we observe a much softer decline in the feature extractor stages and a sharper one in the projector. Representations of CASSLE feature extractor are on average more difficult to match together than those of vanilla MoCo-v2 and AugSelf [37]. This implies that the CASSLE feature extractor is indeed more sensitive to augmentations than its counterparts.

On the other hand, representations of all projectors, including CASSLE, are similarly separable. This suggests that the conditioning mechanism helps CASSLE projector to better amortize the augmentation-induced differences between the feature extractor embeddings.

The above observations indicate that in the vanilla and (to a slightly lesser extent) AugSelf approaches, both the projector and the intermediate representations are enforced to be augmentation-invariant. On the other hand, in CASSLE, the task of augmentation invariance is solved to a larger degree by the projector, and to a smaller degree by the feature extractor, allowing it to be more augmentation-aware. As shown in Section 4.1, this sensitivity does not prevent the CASSLE feature extractor from achieving similar or better performance than its counterparts when transferred to downstream tasks.

Dependency of CASSLE projector on conditioning We next verify that the CASSLE projector indeed relies on the guidance mechanism. In Figure 5, we compare cosine similarities of projector representations of images and augmentation embeddings. We consider true pairs of images and embeddings of augmentations that were applied to them (green), as well as shuffled pairs where the augmentation vector does not correspond to its respective image embedding (red). We can see that incorrect conditioning has a negative effect on the projector, decreasing the similarities of image pairs by a non-trivial margin. This indicates that CASSLE projector indeed depends on augmentation conditioning in order to perform its function well.

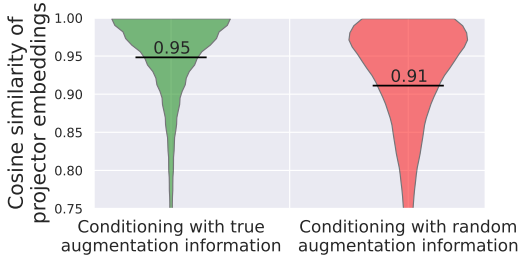


Figure 5: Similarities of CASSLE projector representations when conditioned with augmentation information from either their respective images (green) or other, randomly chosen images (red). Solid lines denote the mean values of similarities. Guiding the CASSLE projector with wrong augmentation information decreases its ability to draw image pairs together, indicating that it indeed relies on augmentation information to perform its task.

4.3 Analysis of the contrastive learning procedure

We next compare the training of MoCo-v2 [32, 14] with and without CASSLE or AugSelf [37] extensions, and plot the contrastive loss values measured throughout training in the left part of Figure 6, and on the right, the values of losses relative to the baseline MoCo-v2. CASSLE minimizes the contrastive objective faster than the other two variants, in particular early in the training procedure. This suggests that augmentation information provides helpful guidance for a model not yet fully trained to align augmented image pairs and thus, CASSLE learns to depend on this information.

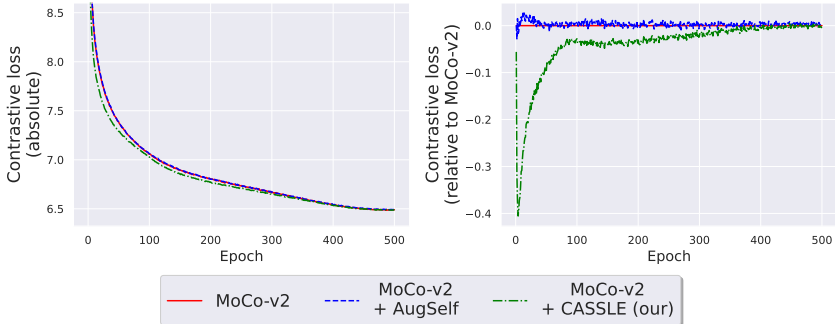


Figure 6: Absolute (left) and relative to Baseline (right) values of contrastive losses of Baseline, AugSelf [37], and CASSLE MoCo-v2 variants, measured during pretraining. CASSLE minimizes the contrastive objective faster than Baseline and AugSelf, in particular early in the training procedure.

4.4 Ablation Study

CASSLE is parametrized by several hyperparameters, described below. To select them optimally, we train different variants of MoCo-v2+CASSLE and evaluate them on the same classification and

Table 3: Ablation study of CASSLE parameters. CASSLE performs best when conditioned on all available augmentation information, by concatenating or adding the augmentation and image embeddings.

Augmentation information	Average rank ↓	Conditioning method	Average rank ↓	Number of layers	Average rank ↓	Hidden size	Average rank ↓
$\omega^{\{c\}}$	3.69	Concatenation	1.92	2	2.77	16	5.54
$\omega^{\{c,j\}}$	3.77	Addition	1.92	4	1.92	32	4.38
$\omega^{\{c,j,d\}}$	2.54	Multiplication	2.69	6	1.77	64	2.54
$\omega^{\{c,j,b,g,f\}}$	2.92	Hypernetwork	3.46	8	3.54	128	2.62
$\omega^{\{c,j,b,g,f,d\}}$	2.15					256	3.31
		(b) Method of conditioning the projector		(c) Guiding network depth		512	2.69
(a) Augmentation information used for guidance						(d) Guiding network hidden size	

regression tasks as in Section 4.1. We rank the models from best to worst performance on each task and report the average ranks in Table 3. We provide the full results in the supplementary material.

Augmentation information contents – We compare conditioning the projector with different subsets of augmentation information. The average best representation is trained with conditioning on all possible augmentation information. Moreover, using the additional **color difference** information additionally improves the results, indicating that it is indeed useful to consider not only augmentation parameters but also information about its effects.

Conditioning the projector – Apart from **concatenation** of image embeddings e and augmentation embeddings g , we consider several other methods of conditioning π with g : element-wise **(2) addition** or **(3) multiplication** of e and g , or **(4) hypernetwork** [28] – generating the parameters of π with γ and processing through π the unmodified e . Conditioning through **concatenation** and **addition** yields on average the strongest performance on downstream tasks. We choose to utilize the **concatenation** method in our experiments, as it requires a slightly smaller Guiding network.

Depth and hidden size of the Guiding Network – While CASSLE is robust to the size of the γ MLP, using the depth and hidden size of 6 and 64, respectively, yields the strongest downstream performance. Given such an architecture of the guiding network, our computation overhead is negligible as we increase the overall number of parameters by around 0.1%.

5 Conclusion

In this paper, we propose a novel method for augmentation-aware self-supervised learning that retains information about data augmentations in the representation space. To accomplish this, we introduce the concept of the guided projector, which receives augmentation information while processing the representation vector. Our solution necessitates only small architectural changes and no additional auxiliary loss components. Therefore, the training concentrates on contrastive loss, which enhances overall performance.

We compare our solution with existing augmentation-aware SSL methods and demonstrate its superior performance on downstream tasks, particularly when augmentation invariance leads to the loss of vital information. Moreover, we show that it converges faster and obtains representations more susceptible to augmentations than the baseline methods.

Overall, our method offers a straightforward and efficient approach for retaining information about data augmentations in the representation space. It can be directly applied to SSL methods, contributing to the further advancement of augmentation-aware self-supervised learning.

Limitations Since our approach relies on modifying the projector network of self-supervised models, such a component must be present in the architecture for CASSLE to be applicable. Recently proposed SSL methods typically meet this requirement [13, 14, 70, 64, 30, 39], but there are others, such as DirectCLR [31], which eliminate the projector and are thus incompatible with CASSLE. Moreover, in CASSLE, the projector is instructed by only parametrized augmentations causing other types of augmentations [16, 19, 18, 69] difficult to encode.

References

- [1] Kumar Krishna Agrawal, Arnab Kumar Mondal, Arna Ghosh, and Blake Aaron Richards. α -req: Assessing representation quality in self-supervised learning by measuring eigenspectrum decay. In Alice H. Oh, Alekh Agarwal, Danielle Belgrave, and Kyunghyun Cho, editors, *Advances in Neural Information Processing Systems*, 2022.
- [2] Saleh Albelwi. Survey on self-supervised learning: Auxiliary pretext tasks and contrastive learning methods in imaging. *Entropy*, 24(4), 2022.
- [3] Haoping Bai, Meng Cao, Ping Huang, and Jiulong Shan. Self-supervised semi-supervised learning for data labeling and quality evaluation, 2021.
- [4] Randall Balestriero, Mark Ibrahim, Vlad Sobal, Ari Morcos, Shashank Shekhar, Tom Goldstein, Florian Bordes, Adrien Bardes, Gregoire Mialon, Yuandong Tian, Avi Schwarzschild, Andrew Gordon Wilson, Jonas Geiping, Quentin Garrido, Pierre Fernandez, Amir Bar, Hamed Pirsiavash, Yann LeCun, and Micah Goldblum. A cookbook of self-supervised learning, 2023.
- [5] Adrien Bardes, Jean Ponce, and Yann LeCun. Vicreg: Variance-invariance-covariance regularization for self-supervised learning, 2022.
- [6] Suzanna Becker and Geoffrey Hinton. Self-organizing neural network that discovers surfaces in random-dot stereograms. *Nature*, 355:161–3, 02 1992.
- [7] Javad Zolfaghari Bengar, Joost van de Weijer, Bartłomiej Twardowski, and Bogdan Raducanu. Reducing label effort: Self-supervised meets active learning. In *Proceedings of the IEEE/CVF International Conference on Computer Vision (ICCV) Workshops*, pages 1631–1639, October 2021.
- [8] Florian Bordes, Randall Balestriero, Quentin Garrido, Adrien Bardes, and Pascal Vincent. Guillotine regularization: Improving deep networks generalization by removing their head, 2022.
- [9] Lukas Bossard, Matthieu Guillaumin, and Luc Van Gool. Food-101 – mining discriminative components with random forests. In *European Conference on Computer Vision*, 2014.
- [10] Tom Brown, Benjamin Mann, Nick Ryder, Melanie Subbiah, Jared D Kaplan, Prafulla Dhariwal, Arvind Neelakantan, Pranav Shyam, Girish Sastry, Amanda Askell, et al. Language models are few-shot learners. *Advances in neural information processing systems*, 33:1877–1901, 2020.
- [11] Mathilde Caron, Hugo Touvron, Ishan Misra, Hervé Jégou, Julien Mairal, Piotr Bojanowski, and Armand Joulin. Emerging properties in self-supervised vision transformers. In *Proceedings of the International Conference on Computer Vision (ICCV)*, 2021.
- [12] Ruchika Chavhan, Henry Gouk, Jan Stuehmer, Calum Heggan, Mehrdad Yaghoobi, and Timothy Hospedales. Amortised invariance learning for contrastive self-supervision, 2023.
- [13] Ting Chen, Simon Kornblith, Mohammad Norouzi, and Geoffrey Hinton. A simple framework for contrastive learning of visual representations, 2020.
- [14] Xinlei Chen, Haoqi Fan, Ross Girshick, and Kaiming He. Improved baselines with momentum contrastive learning, 2020.
- [15] Xinlei Chen, Saining Xie, and Kaiming He. An empirical study of training self-supervised vision transformers, 2021.
- [16] Kaiyang Cheng, Claudia Iriondo, Francesco Calivá, Justin Krogue, Sharmila Majumdar, and Valentina Pedoia. Adversarial policy gradient for deep learning image augmentation, 2019.
- [17] M. Cimpoi, S. Maji, I. Kokkinos, S. Mohamed, , and A. Vedaldi. Describing textures in the wild. In *Proceedings of the IEEE Conf. on Computer Vision and Pattern Recognition (CVPR)*, 2014.
- [18] Ekin D. Cubuk, Barret Zoph, Dandelion Mane, Vijay Vasudevan, and Quoc V. Le. Autoaugment: Learning augmentation policies from data, 2019.
- [19] Ekin D. Cubuk, Barret Zoph, Jonathon Shlens, and Quoc V. Le. Randaugment: Practical automated data augmentation with a reduced search space, 2019.
- [20] Jacob Devlin, Ming-Wei Chang, Kenton Lee, and Kristina Toutanova. Bert: Pre-training of deep bidirectional transformers for language understanding, 2019.
- [21] Carl Doersch, Abhinav Gupta, and Alexei A. Efros. Unsupervised visual representation learning by context prediction. *CoRR*, abs/1505.05192, 2015.
- [22] Alexey Dosovitskiy, Lucas Beyer, Alexander Kolesnikov, Dirk Weissenborn, Xiaohua Zhai, Thomas Unterthiner, Mostafa Dehghani, Matthias Minderer, Georg Heigold, Sylvain Gelly, Jakob Uszkoreit, and Neil Houlsby. An image is worth 16x16 words: Transformers for image recognition at scale, 2021.
- [23] Linus Ericsson, Henry Gouk, and Timothy M. Hospedales. Why do self-supervised models transfer? investigating the impact of invariance on downstream tasks, 2022.

- [24] M. Everingham, L. Van Gool, C. K. I. Williams, J. Winn, and A. Zisserman. The PASCAL Visual Object Classes Challenge 2007 (VOC2007) Results. <http://www.pascal-network.org/challenges/VOC/voc2007/workshop/index.html>.
- [25] Li Fei-Fei, R. Fergus, and P. Perona. One-shot learning of object categories. *IEEE Transactions on Pattern Analysis and Machine Intelligence*, 28(4):594–611, 2006.
- [26] Spyros Gidaris, Praveer Singh, and Nikos Komodakis. Unsupervised representation learning by predicting image rotations, 2018.
- [27] Ian Goodfellow, Yoshua Bengio, and Aaron Courville. *Deep learning*. MIT press, 2016.
- [28] David Ha, Andrew Dai, and Quoc V. Le. Hypernetworks, 2016.
- [29] Kaiming He, Xiangyu Zhang, Shaoqing Ren, and Jian Sun. Deep residual learning for image recognition, 2015.
- [30] Grill J.-B. et al. Bootstrap your own latent: A new approach to self-supervised learning. In *NeurIPS*, 2020.
- [31] Li Jing, Pascal Vincent, Yann LeCun, and Yuandong Tian. Understanding dimensional collapse in contrastive self-supervised learning. In *International Conference on Learning Representations*, 2022.
- [32] He K. et al. Momentum contrast for unsupervised visual representation learning. In *CVPR*, 2020.
- [33] Tae Soo Kim, Geonwoon Jang, Sanghyup Lee, and Thijs Kooi. Did you get what you paid for? rethinking annotation cost of deep learning based computer aided detection in chest radiographs, 2022.
- [34] Simon Kornblith, Jonathon Shlens, and Quoc V. Le. Do better imagenet models transfer better?, 2019.
- [35] Jonathan Krause, Michael Stark, Jia Deng, and Li Fei-Fei. 3d object representations for fine-grained categorization. In *4th International IEEE Workshop on 3D Representation and Recognition (3dRR-13)*, Sydney, Australia, 2013.
- [36] Alex Krizhevsky. Learning multiple layers of features from tiny images. 2009.
- [37] Hankook Lee, Kibok Lee, Kimin Lee, Honglak Lee, and Jinwoo Shin. Improving transferability of representations via augmentation-aware self-supervision. *CoRR*, abs/2111.09613, 2021.
- [38] Tsung-Yi Lin, Michael Maire, Serge J. Belongie, Lubomir D. Bourdev, Ross B. Girshick, James Hays, Pietro Perona, Deva Ramanan, Piotr Dollár, and C. Lawrence Zitnick. Microsoft COCO: common objects in context. *CoRR*, abs/1405.0312, 2014.
- [39] Caron M. et al. Unsupervised learning of visual features by contrasting cluster assignments. In *NeurIPS*, 2020.
- [40] Subhransu Maji, Esa Rahtu, Juho Kannala, Matthew Blaschko, and Andrea Vedaldi. Fine-grained visual classification of aircraft, 2013.
- [41] Grégoire Mialon, Randall Balestriero, and Yann LeCun. Variance covariance regularization enforces pairwise independence in self-supervised representations, 2022.
- [42] Volodymyr Mnih, Koray Kavukcuoglu, David Silver, Andrei A Rusu, Joel Veness, Marc G Bellemare, Alex Graves, Martin Riedmiller, Andreas K Fidjeland, Georg Ostrovski, et al. Human-level control through deep reinforcement learning. *nature*, 518(7540):529–533, 2015.
- [43] Sharada Prasanna Mohanty, David Hughes, and Marcel Salathe. Using deep learning for image-based plant disease detection, 2016.
- [44] Maria-Elena Nilsback and Andrew Zisserman. Automated flower classification over a large number of classes. In *Indian Conference on Computer Vision, Graphics and Image Processing*, Dec 2008.
- [45] Mehdi Noroozi and Paolo Favaro. Unsupervised learning of visual representations by solving jigsaw puzzles, 2017.
- [46] Maxime Oquab, Timothée Darcet, Théo Moutakanni, Huy Vo, Marc Szafraniec, Vasil Khalidov, Pierre Fernandez, Daniel Haziza, Francisco Massa, Alaaeldin El-Nouby, Mahmoud Assran, Nicolas Ballas, Wojciech Galuba, Russell Howes, Po-Yao Huang, Shang-Wen Li, Ishan Misra, Michael Rabbat, Vasu Sharma, Gabriel Synnaeve, Hu Xu, Hervé Jegou, Julien Mairal, Patrick Labatut, Armand Joulin, and Piotr Bojanowski. Dinov2: Learning robust visual features without supervision, 2023.
- [47] Boris N. Oreshkin, Pau Rodriguez, and Alexandre Lacoste. Tadam: Task dependent adaptive metric for improved few-shot learning, 2019.
- [48] Omkar M. Parkhi, Andrea Vedaldi, Andrew Zisserman, and C. V. Jawahar. Cats and dogs. In *IEEE Conference on Computer Vision and Pattern Recognition*, 2012.
- [49] Adam Paszke, Sam Gross, Francisco Massa, Adam Lerer, James Bradbury, Gregory Chanan, Trevor Killeen, Zeming Lin, Natalia Gimelshein, Luca Antiga, Alban Desmaison, Andreas Kopf, Edward Yang, Zachary DeVito, Martin Raison, Alykhan Tejani, Sasank Chilamkurthy, Benoit Steiner, Lu Fang, Junjie Bai, and Soumith Chintala. Pytorch: An imperative style, high-performance deep learning library. In *Advances in Neural Information Processing Systems 32*, pages 8024–8035. Curran Associates, Inc., 2019.

- [50] F. Pedregosa, G. Varoquaux, A. Gramfort, V. Michel, B. Thirion, O. Grisel, M. Blondel, P. Prettenhofer, R. Weiss, V. Dubourg, J. Vanderplas, A. Passos, D. Cournapeau, M. Brucher, M. Perrot, and E. Duchesnay. Scikit-learn: Machine learning in Python. *Journal of Machine Learning Research*, 12:2825–2830, 2011.
- [51] Ariadna Quattoni and Antonio Torralba. Recognizing indoor scenes. In *2009 IEEE Conference on Computer Vision and Pattern Recognition*, pages 413–420, 2009.
- [52] Aniruddh Raghu, Jonathan Lorraine, Simon Kornblith, Matthew McDermott, and David K Duvenaud. Meta-learning to improve pre-training. In M. Ranzato, A. Beygelzimer, Y. Dauphin, P.S. Liang, and J. Wortman Vaughan, editors, *Advances in Neural Information Processing Systems*, volume 34, pages 23231–23244. Curran Associates, Inc., 2021.
- [53] Olga Russakovsky, Jia Deng, Hao Su, Jonathan Krause, Sanjeev Satheesh, Sean Ma, Zhiheng Huang, Andrej Karpathy, Aditya Khosla, Michael Bernstein, Alexander C. Berg, and Li Fei-Fei. Imagenet large scale visual recognition challenge, 2015.
- [54] Ren S. et al. Faster r-cnn: Towards real-time object detection with region proposal networks. In *NeurIPS*, 2015.
- [55] C. Sagonas, E. Antonakos, Tzimiropoulos G, S. Zafeiriou, and M. Pantic. 300 faces in-the-wild challenge: Database and results. In *Image and Vision Computing (IMAVIS), Special Issue on Facial Landmark Localisation*, 2016.
- [56] Madeline C. Schiappa, Yogesh S. Rawat, and Mubarak Shah. Self-supervised learning for videos: A survey. *ACM Computing Surveys*, dec 2022.
- [57] Yisheng Song, Ting Wang, Subrota K Mondal, and Jyoti Prakash Sahoo. A comprehensive survey of few-shot learning: Evolution, applications, challenges, and opportunities, 2022.
- [58] Yonglong Tian, Chen Sun, Ben Poole, Dilip Krishnan, Cordelia Schmid, and Phillip Isola. What makes for good views for contrastive learning? *arXiv preprint arXiv:2005.10243*, 2020.
- [59] Yuandong Tian. Understanding deep contrastive learning via coordinate-wise optimization, 2022.
- [60] Aaron van den Oord, Yazhe Li, and Oriol Vinyals. Representation learning with contrastive predictive coding, 2019.
- [61] Diane Wagner, Fábio Ferreira, Danny Stoll, Robin Tibor Schirrmeyer, Samuel G. Müller, and Frank Hutter. On the importance of hyperparameters and data augmentation for self-supervised learning. *ArXiv*, abs/2207.07875, 2022.
- [62] C. Wah, S. Branson, P. Welinder, P. Perona, and S. Belongie. The Caltech-UCSD Birds-200-2011 Dataset. Technical Report CNS-TR-2011-001, California Institute of Technology, 2011.
- [63] Kristoffer Wickstrøm, Michael Kampffmeyer, Karl Øyvind Mikalsen, and Robert Jenssen. Mixing up contrastive learning: Self-supervised representation learning for time series. *Pattern Recognition Letters*, 155:54–61, mar 2022.
- [64] Chen X. and He K. Exploring simple siamese representation learning. In *CVPR*, 2021.
- [65] J. Xiao, J. Hays, K. A. Ehinger, A. Oliva, and A. Torralba. Sun database: Large-scale scene recognition from abbey to zoo. In *2010 IEEE Computer Society Conference on Computer Vision and Pattern Recognition*, pages 3485–3492, June 2010.
- [66] Tete Xiao, Xiaolong Wang, Alexei A. Efros, and Trevor Darrell. What should not be contrastive in contrastive learning, 2020.
- [67] Yuyang Xie, Jianhong Wen, Kin Wai Lau, Yasar Abbas Ur Rehman, and Jiajun Shen. What should be equivariant in self-supervised learning. In *Proceedings of the IEEE/CVF Conference on Computer Vision and Pattern Recognition (CVPR) Workshops*, pages 4111–4120, June 2022.
- [68] Jason Yosinski, Jeff Clune, Yoshua Bengio, and Hod Lipson. How transferable are features in deep neural networks?, 2014.
- [69] Sangdoon Yun, Dongyoon Han, Seong Joon Oh, Sanghyuk Chun, Junsuk Choe, and Youngjoon Yoo. Cutmix: Regularization strategy to train strong classifiers with localizable features, 2019.
- [70] Jure Zbontar, Li Jing, Ishan Misra, Yann LeCun, and Stéphane Deny. Barlow twins: Self-supervised learning via redundancy reduction, 2021.
- [71] Richard Zhang, Phillip Isola, and Alexei A. Efros. Colorful image colorization, 2016.
- [72] Simone Zini, Alex Gomez-Villa, Marco Buzzelli, Bartłomiej Twardowski, Andrew D. Bagdanov, and Joost van de Weijer. Planckian jitter: countering the color-crippling effects of color jitter on self-supervised training, 2023.

A Pretraining details

A.1 Datasets

We use ImageNet-100, a 100-class subset of ImageNet [53, 58], to pretrain the standard ResNet-50 [29] architecture of self-supervised methods: MoCo-v2 [14], SimCLR [13], Barlow Twins [70], and SimSiam [64], as well as for common in the literature on augmentation-aware self-supervised learning [58, 66, 37, 12]. For MoCo-v3 [15], we pretrain the ViT-Small [22] model on the full ImageNet dataset [53].

A.2 Hyperparameters

We follow the pretraining procedures from corresponding papers, described in [37] for MoCo-v2 and SimSiam, [12] for SimCLR, [70] for Barlow Twins, and [15] for MoCo-v3. CASSLE is trained with ResNet50 and ViT-small architectures on 2 and 8 NVidia A100 GPUs, respectively. Synchronized batch normalization is employed for distributed training [64]. In Table 4, we present the training hyperparameters which are not related specifically to CASSLE, but rather joint-embedding approaches in general [32, 14, 13, 70, 64, 15].

Table 4: Hyperparameters of self-supervised methods used with CASSLE

SSL method	Architecture	Number of epochs	Batch size	Weight decay	Learning rate		Training time
					Base	Schedule	
MoCo-v2 [14]	ResNet-50	500	256	10^{-4}	0.03	Cosine decay	34h
SimCLR [13]	ResNet-50	300	256	10^{-4}	0.05	Cosine decay	48h
Barlow Twins [70]	ResNet-50	500	256	10^{-4}	0.05	Cosine decay with warmup	36h
SimSiam [64]	ResNet-50	500	256	10^{-4}	0.05	Cosine decay	40h
MoCo-v3 [15]	ViT-small	300	1024	0.1	$1.5 \cdot 10^{-4}$	Cosine decay with warmup	23h

SSL method	Projector				Predictor			
	Depth	Hidden size	Out size	Final BatchNorm	Depth	Hidden size	Out size	Final BatchNorm
MoCo-v2 [14]	2	2048	128	No				No
SimCLR [13]	2	2048	128	No				No
Barlow Twins [70]	3	8192	8192	Yes, without affine transform				No
SimSiam [64]	3	2048	2048	Yes	2	512	2048	No
MoCo-v3 [15]	3	4096	256	Yes, without affine transform	2	4096	256	Yes, without affine transform

A.3 Augmentations

For self-supervised pretraining, we use a set of augmentations adopted commonly in the literature [32, 13, 14, 64, 70, 37]. We denote them below:

- **random cropping** – We sample the cropping scale randomly from [0.2, 1.0]. Afterward, we resize the cropped images to the size of 224×224 .
- **color jittering** – We apply this operation with a probability of 0.8. We sample the intensities of brightness, contrast, saturation, and hue and their maximal values are 0.4, 0.4, 0.4, and 0.1, respectively.
- **Gaussian blurring** – We apply this operation with a probability of 0.5. We sample the standard deviation from [0.1, 2.0] and set the kernel size to 23×23 .
- **random horizontal flipping** – We apply this operation with a probability of 0.5.
- **random grayscaling** – We apply this operation with a probability of 0.2.

B Evaluation protocol

B.1 Datasets

We outline the datasets and their respective evaluation metrics used for downstream tasks that we evaluate CASSLE on in Table 5.

Table 5: Information about datasets and their metrics used for downstream evaluation of CASSLE.

Downstream task	Dataset	Metric
Linear evaluation	CIFAR10 [36]	Top-1 accuracy
	CIFAR100 [36]	Top-1 accuracy
	Food101 [9]	Top-1 accuracy
	MIT67 [51]	Top-1 accuracy
	Oxford-IIIT Pets [48]	Mean per-class accuracy
	Oxford Flowers-102 [44]	Mean per-class accuracy
	Caltech101 [25]	Mean per-class accuracy
	Stanford Cars [35]	Top-1 accuracy
	FGVC-Aircraft [40]	Mean Per-class accuracy
	Describable Textures (split 1) [17]	Top-1 accuracy
	SUN397 (split 1) [65]	Top-1 accuracy
Caltech-UCSD Birds [62]	Top-1 accuracy	
300 Faces In-the-Wild [55]	R^2	
Object detection	VOC2007 [24]	Average Precision [38]
Few-shot classification	Few-Shot CIFAR100 [47]	Average accuracy
	Caltech-UCSD Birds [62]	Average accuracy
	Plant Disease [43]	Average accuracy
	Oxford Flowers-102 [44]	Mean per-class accuracy

Linear evaluation We follow the linear evaluation protocol of [13, 30, 34, 37]. Namely, we center-crop and resize the images from the downstream dataset to the size of 224×224 , pass them through the pretrained feature extractor, and obtain the embeddings from the final feature extractor stage. The only exception from this is the CUB dataset [62], where, following [37], for the training images besides the center crop of the image, we also crop the image at its corners and do the same for the horizontal flip of the image (this is known as TenCrop operation⁵).

Having gathered the image features, we minimize the l_2 -regularized cross-entropy objective using L-BFGS on the features of the training images. We select the regularization parameter from between $[10^{-6}, 10^5]$ using the validation features. Finally, we train the linear classifier on training and validation features with the selected l_2 parameter and report the final performance metric (see Table 5) on the test dataset. We set the maximum number of iterations in L-BFGS as 5000 and use the model trained on training data as initialization for training the final model.

We note that the above linear evaluation procedure is effectively equivalent to training the final layer of a network on non-augmented data, while keeping the remainder of the parameters unchanged.

Few-shot evaluation We follow the evaluation protocol of [37]. For the task of 5/10-shot learning of the Flowers dataset [44], we select the subset of the training set with 5/10 examples per class, respectively, and utilize the linear evaluation protocol presented above. For the remaining datasets used for few-shot evaluation, we extract the representations of support and query images with the feature extractor and train a logistic regression model⁶, which we evaluate on the query set. We report the average accuracy from 2000 N -way K -shot tasks [57].

Object detection We closely follow the evaluation protocol of [32]. We train the Faster-RCNN [54] model with the pretrained backbone. Contrary to [32], we do not tune the backbone parameters, in order to better observe the effect of different pretraining methods. We report the Average Precision [38] measured on the VOC test2007 set [24].

Image retrieval We gather the features of images from downstream test sets and for a given query image, select 4 images closest to it in terms of the cosine distance of final feature extractor features.

⁵<https://pytorch.org/vision/main/generated/torchvision.transforms.TenCrop.html>

⁶We use the LogisticRegression implementation from scikit-learn [50].

Table 6: Linear evaluation on downstream task: predicting the rotation (0, 90, 180 or 270 degrees)

Method	C10	C100	Food	Pets	MIT	Flowers	Caltech	Cars	FGVCA	STL10	SUN
<i>SimCLR</i> [13]											
Vanilla	67.93	56.88	68.76	65.07	70.40	24.15	56.81	87.12	98.02	73.90	67.94
AugSelf [37]	75.63	63.08	75.01	57.99	16.54	33.99	39.03	76.11	96.64	67.88	76.60
CASSLE	77.07	70.20	79.55	70.97	68.77	33.08	64.97	95.14	99.46	72.69	78.16
<i>MoCo-v2</i> [32, 14]											
Vanilla	67.96	56.96	75.70	71.27	67.13	58.30	87.33	58.35	93.20	95.44	68.33
AugSelf [37]	74.57	65.87	73.03	77.01	79.75	52.81	58.53	93.07	98.26	77.35	83.66
CASSLE	73.21	69.91	77.31	76.04	76.40	45.11	61.06	90.49	98.56	63.65	76.01
<i>SimSiam</i> [64]											
Vanilla	68.11	64.81	77.35	61.79	79.10	46.33	64.76	80.50	97.48	55.38	74.49
AugSelf [37]	77.00	72.91	73.03	59.18	78.28	49.11	60.86	97.21	99.46	76.68	83.14
CASSLE	72.00	71.38	78.01	85.30	66.80	37.65	61.64	92.04	98.65	63.69	75.86
<i>Barlow Twins</i> [70]											
Vanilla	73.67	64.87	72.85	83.02	70.97	42.56	57.71	83.68	97.93	65.70	76.87
AugSelf [37]	72.79	65.91	74.93	77.76	50.30	30.93	44.31	85.85	98.35	69.68	77.19
CASSLE	74.97	65.15	76.55	77.05	86.49	43.16	53.60	92.92	99.16	55.24	74.97

Sensitivity to augmentations We consider image pairs, where one image is the (center-cropped) original and the second one is augmented by the given augmentation. For each image pair, we extract image features at four stages of the pretrained ResNet-50 backbone [29], as well as the final representation of the projector network. We next calculate cosine similarities between the features of augmented and non-augmented images in the given mini-batch (of size 256). We report the value of the InfoNCE loss [60] calculated on such similarity matrices.

Dependency of CASSLE projector on conditioning Similarly to the above experiment, we compare the projector features of augmented and non-augmented image pairs. When computing the features of the augmented image, we supply the projector with the augmentation embedding computed from augmentation parameters corresponding to either this image (true augmentation information) or another, randomly chosen image from the same mini-batch (random augmentation information). We then compute cosine similarities between the original image features and features of the augmented image computed with true/random augmentation information.

C Additional results and analysis

Rotation prediction In order to understand whether CASSLE learns to generalize to other types of augmentation, which were not used during pretraining, we inspect the prediction of applied augmentation through the following experiment. We train a linear classifier on top of the pretrained model to indicate whether the image was rotated by 0, 90, 180, or 270 degrees. We formulate the problem as classification due to its cyclic nature and test the model on the datasets used for linear evaluation in Section 4.1 of the main manuscript. We present the results of vanilla, AugSelf [37] and CASSLE variants of self-supervised methods in Table 6.

Apart from a few exceptions, CASSLE and AugSelf extensions allow in general for better prediction of rotation than the vanilla SSL methods. Moreover, in the case of SimCLR, CASSLE representation predicts the rotations the most accurately on a vast majority of datasets. This occurs despite the fact, that neither of the methods was trained using rotated images and thus, never explicitly learned the *concept* of rotation. This suggests that CASSLE learns representations which are sensitive to a broader set of perturbations than those whose information had been used in CASSLE’s pretraining.

Analysis of dimensional collapse of representations Augmentation-invariant SSL models are known to suffer from dimensional collapse of their representations, due to the usage of strong augmentations and implicit regularization [31]. Here, we analyze the effect of CASSLE on this

phenomenon. To this end, we compute the embeddings of the ImageNet-100 test dataset with pretrained feature extractors and calculate the empirical eigenspectra of the embeddings produced by each encoder. We next analyze the power-law decay rates (α) of eigenspectra [1]. Intuitively, smaller values of α suggest a dense encoding, while larger values of α suggest more sparse encoding and rapid decay. We report the calculated coefficients in Table 7. In all analyzed SSL methods, except Barlow Twins, the addition of augmentation information by CASSLE leads to a representation whose eigenspectrum decays more rapidly, thus suggesting a lower rank of the effective embedding subspace and as such, greater dimensional collapse. However, as seen in Section 4.1 of the main text, this does not necessarily lead to degraded performance – indeed, performance on downstream tasks has been previously correlated with how close α is to 1 [1].

Table 7: Power-law eigenspectrum decay rates (α) [1] of embeddings of ImageNet-100 test set produced by differently pretrained feature extractors.

Method	MoCo-v2 [32, 14]	SimCLR [13]	Barlow Twins [70]	SimSiam [64]
Vanilla	0.6013	0.6150	0.5387	0.6365
AugSelf [37]	0.6146	0.6251	0.5201	0.6262
CASSLE	0.6342	0.6908	0.5196	0.6962

We illustrate this further with a Principal Component Analysis of features extracted by different variants of joint-embedding methods illustrated in Figure 7. We extract embeddings of the test ImageNet-100 images and calculate the ratio of variance explained by principal components of embeddings. We find that, in general, representations learned with CASSLE require fewer principal components to explain larger amounts of variance. For example, for MoCo-v2, 90% of variance is explained by 905, 872, and 736 principal components of representations learned by the vanilla approach, AugSelf [37], and CASSLE, respectively. This again suggests that representations learned by CASSLE have lower effective rank compared to other approaches.

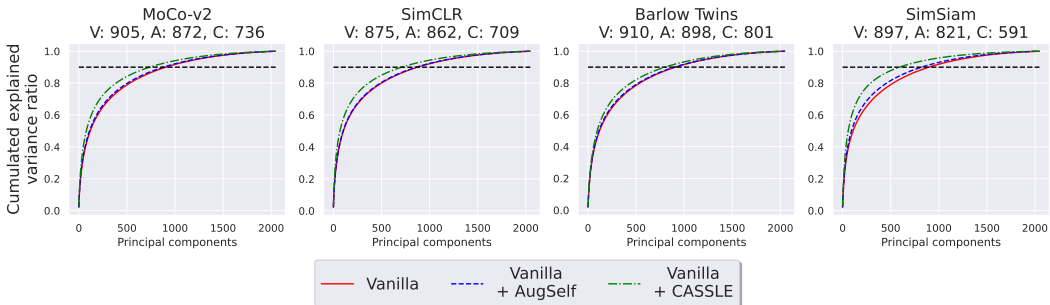


Figure 7: Cumulated explained variance ratio of representations learned by self-supervised models trained in their original forms, as well as with AugSelf [37] and CASSLE extensions. We additionally denote the number of principal components which that explain 90% of variance of each representation. Models pretrained with CASSLE explain the largest amount of variance with the smallest amount of components, suggesting a larger dimensionality collapse of their representations.

Few-shot classification We next benchmark various forms of pretraining on a number of few-shot learning tasks: Few-Shot CIFAR100 (FC100) [47], Caltech-UCSD Birds (CUB) [62], Plant Disease [43]. For the above datasets, we report the performance on 5-way 1-shot and 5-way 5-shot tasks. Moreover, we also report the performance on the 5-shot and 10-shot versions of the Flowers-102 dataset (Flowers) [44]. Following [37], our few-shot models are trained through logistic regression on representations of support images, without fine-tuning. We report the results in Table 8. In general, CASSLE improves the performance of the vanilla joint-embedding approaches, but to a lesser extent than AugSelf [37] or AI [12]. The notable exception is Barlow Twins [70], where CASSLE yields the strongest performance boost.

Image retrieval In Figures 8 and 9, we present additional image retrieval examples of MoCo-v2, AugSelf [37], and CASSLE on Cars and Flowers datasets. CASSLE and AugSelf retrieve in general more consistently looking images, in particular in terms of color scheme. However, for some distinct

Table 8: Few-shot classification accuracy averaged over 2000 tasks on Few-Shot CIFAR100 (FC100) [47], Caltech-UCSD Birds (CUB) [62], Plant Disease [43], and accuracy on 5-shot and 10-shot versions of Flowers-102 dataset (Flowers) [44]. (N, K) denotes N-way K-shot tasks. The best performance in each group is **bolded**.

Method	FC100		CUB		Plant Disease		Flowers	
	(5,1)	(5,5)	(5,1)	(5,5)	(5,1)	(5,5)	(102, 5)	(102,10)
<i>MoCo v2</i> [32, 14]								
Vanilla	31.67	43.88	41.67	56.92	65.73	84.98	66.83 [†]	78.80 [†]
AugSelf [37]	35.02	48.77	44.17	57.35	71.80	87.81	72.95[†]	82.12[†]
AI [12]	37.40	48.40	45.00	58.00	72.60	89.10	–	–
LooC [66]	–	–	–	–	–	–	70.90	80.80
CASSLE	35.15	49.30	42.98	55.82	70.74	87.12	72.36	82.07
<i>SimCLR</i> [13]								
Vanilla [†]	32.47	44.46	40.83	53.58	70.82	87.53	70.73	80.72
AugSelf [37] [†]	36.72	49.15	42.80	57.08	73.85	89.46	73.86	82.91
CASSLE	34.24	47.34	41.26	55.98	73.89	89.20	73.23	83.34
<i>Barlow Twins</i> [70]								
Vanilla [†]	38.08	53.93	43.20	61.95	70.98	91.06	75.28	83.43
AugSelf [37] [†]	37.48	54.16	42.50	61.86	71.28	91.16	74.49	83.62
CASSLE	38.58	54.03	43.22	62.65	73.47	92.17	76.62	85.50
<i>SimSiam</i> [64]								
Vanilla	36.19	50.36	45.56	62.48	75.72	89.94	75.53 [†]	85.90
AugSelf [37]	39.37	55.27	48.08	66.27	77.93	91.52	79.67[†]	88.30
CASSLE	36.18	50.16	44.93	60.07	76.43	90.82	77.96	86.64

images, such as the last presented image of flowers, all methods have retrieved the correct results for the given query.

Theoretical motivation for CASSLE We present an informal rationale for why CASSLE preserves the information about the applied augmentation in the output of feature extractor f . If the feature extractor f yields augmentation-invariant representation, then the embeddings $f(\mathbf{v}_1) = \mathbf{e}_1, f(\mathbf{v}_2) = \mathbf{e}_2$ would have comparable representations, i.e. $\mathbf{e}_2 \cong \mathbf{e}_1$. This scenario is detrimental for minimizing the contrastive loss $\mathcal{L}(\pi(\mathbf{e}_1, \mathbf{g}_1), \pi(\mathbf{e}_2, \mathbf{g}_2))$ because we provide the projector π with supplementary input indicating the augmentation. If \mathbf{g}_1 differs from \mathbf{g}_2 and π is non-trivial, then for contrastive loss reduction the embedding \mathbf{e}_i should incorporate information pertaining to the augmentation \mathbf{g}_i . We refer to experimental results presented in Section 4.2 of the main manuscript, where this phenomenon is verified experimentally.

Ablation study In order to optimally select the hyperparameters of CASSLE, we train different variants of MoCo-v2+CASSLE and evaluate them on the same classification and regression tasks as in Section 4.1 of the main paper. We rank the models from best to worst performance on each task and report the full results and average ranks in Table 9.

We recall the notation used for Augmentation information contents – $\omega^{\{x,y\}}$ denotes including parameters of augmentations $\{x, y\}$ in augmentation information vector ω . For example, $\omega^{\{c,j\}}$ denotes ω containing cropping and color jittering parameters.

D Implementation details

We implement CASSLE in the PyTorch framework [49], building upon the codebase of Lee et. al. [37]. Our code is available at <https://github.com/gmum/CASSLE>.

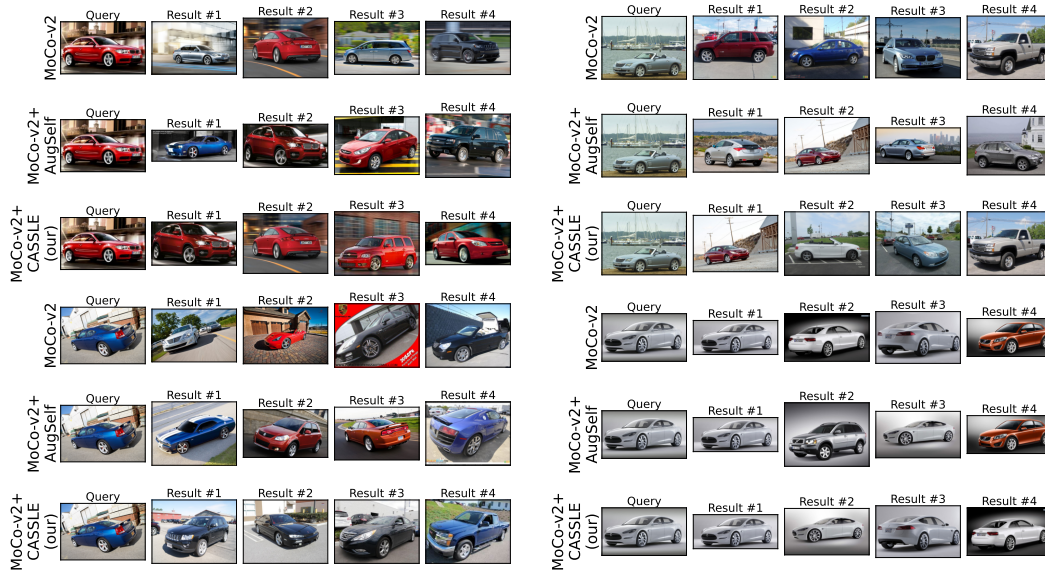


Figure 8: Image retrieval on Cars dataset

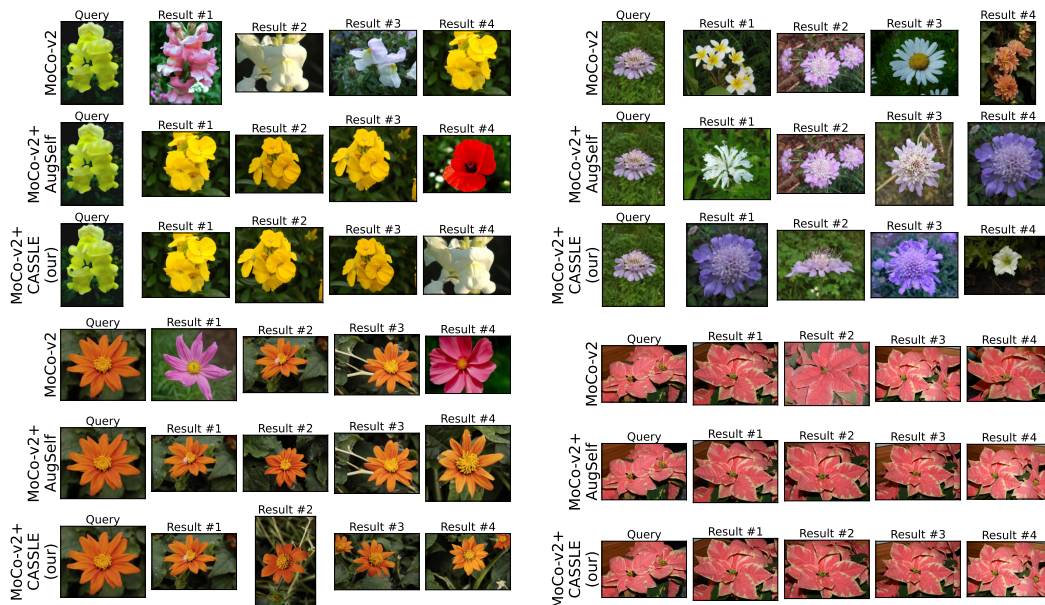


Figure 9: Image retrieval on Flowers dataset

Table 9: Ablation study of CASSLE parameters. The results are computed with MoCo-v2+CASSLE. It is best to condition CASSLE on all available augmentation information. CASSLE yields the best results when implemented by concatenating or adding the augmentation and image embeddings together.

Parameter	C10	C100	Food	MIT	Pets	Flowers	Caltech	Cars	FGVCA	DTD	SUN	CUB	300W	Average rank ↓
Augmentation information contents														
$\omega^{\{c\}}$	84.89	62.95	59.74	63.96	72.26	83.55	79.66	38.78	42.03	65.11	48.44	33.86	89.17	3.69
$\omega^{\{c,j\}}$	85.56	64.26	60.35	62.61	71.97	84.73	79.86	38.13	42.17	66.28	48.01	34.24	88.76	3.77
$\omega^{\{c,j,d\}}$	85.87	63.91	61.07	63.51	72.71	86.53	79.51	38.27	42.53	66.70	49.27	35.76	89.11	2.54
$\omega^{\{c,j,b,g,f\}}$	85.85	64.14	61.24	63.73	72.88	84.50	79.93	38.23	41.28	65.27	48.90	34.47	88.78	2.92
$\omega^{\{c,j,b,g,f,d\}}$	86.99	65.28	61.83	63.51	73.22	86.55	79.87	37.97	41.70	67.18	48.85	36.92	89.03	2.15
Conditioning of projector														
Concatenation	86.99	65.28	61.83	63.51	73.22	86.55	79.87	37.97	41.70	67.18	48.85	36.92	89.03	1.92
Addition	86.45	65.40	63.00	65.15	71.34	86.91	79.79	37.83	42.18	66.17	49.28	37.42	88.87	1.92
Multiplication	86.72	66.70	60.65	60.97	64.60	85.17	80.09	33.54	41.56	63.99	47.63	32.15	89.48	2.69
Hypernetwork	84.70	63.55	60.62	64.10	67.16	82.76	78.47	33.39	39.85	66.44	47.43	30.48	89.11	3.46
Depth of guiding network														
2	86.57	64.80	61.85	62.68	72.79	86.31	79.93	37.85	42.87	66.32	49.23	35.39	88.86	2.77
4	86.32	65.16	61.98	64.93	72.64	86.49	79.75	38.64	41.46	66.91	49.71	36.56	89.27	1.92
6	86.99	65.28	61.83	63.51	73.22	86.55	79.87	37.97	41.70	67.18	48.85	36.92	89.03	1.77
8	85.47	64.88	61.49	63.13	72.41	85.65	78.22	37.82	40.71	66.70	49.21	36.09	88.90	3.54
Hidden size of guiding network														
16	84.51	63.40	61.38	62.31	71.61	85.40	78.96	37.53	41.84	66.54	48.68	35.54	88.78	5.54
32	85.43	63.94	61.93	64.18	72.05	85.67	79.80	37.86	41.52	67.13	48.71	35.64	88.67	4.38
64	86.99	65.28	61.83	63.51	73.22	86.55	79.87	37.97	41.70	67.18	48.85	36.92	89.03	2.54
128	86.24	64.66	61.95	64.25	72.12	86.72	79.56	37.79	42.71	67.61	49.52	36.87	88.99	2.62
256	86.23	65.63	61.77	61.79	72.03	85.69	80.38	37.86	40.94	67.07	49.59	37.00	89.37	3.31
512	85.77	66.05	62.21	64.55	72.45	86.38	80.06	37.91	41.94	66.22	49.35	36.24	88.87	2.69